This is a preprint, the final version is subject to change, of the American Mineralogist (MSA)
Cite as Authors (Year) Title. American Mineralogist, in press.
DOI: https://doi.org/10.2138/am-2020-6988

REVISION 3

^{222}Rn and ^{220}Rn emanations from powdered samples of samarskite as a function of annealing temperature

Dariusz Malczewski

Faculty of Earth Sciences, University of Silesia, Bedzinska 60, 41-200 Sosnowiec, Poland

e-mail: dariusz.malczewski@us.edu.pl

Maria Dziurowicz

Faculty of Earth Sciences, University of Silesia, Bedzinska 60, 41-200 Sosnowiec, Poland

e-mail: maria.dziurowicz@us.edu.pl

ABSTRACT

Emanation coefficients for radon (^{222}Rn) and thoron (^{220}Rn) were measured from fully metamict samarskite collected from Centennial Cone after 1 h and 24 h annealing in argon from 473 to 1373 K. For the 1 h annealing run, ^{222}Rn emanation coefficients ranged from 5 x 10^{-6} to 2.1 x 10^{-5} %, while ^{220}Rn coefficients varied from 6.3 x 10^{-3} to 2 x 10^{-2} %. For the 24 h annealing run, ^{222}Rn coefficients ranged from 5.8 x 10^{-6} to 2.3 x 10^{-5} %, while ^{220}Rn coefficients varied from 4.1 x 10^{-3} to 1.5 x 10^{-2} %. The ^{222}Rn and ^{220}Rn emanation coefficients versus annealing temperature data can be described by an exponentially decreasing sinusoidal function. Both ^{222}Rn and ^{220}Rn emanation coefficient values after annealing considerably exceeded those measured from an unheated powder reference sample and from the original samarskite sample.

Keywords: samarskite, radon emanations, thoron emanations, recrystallization, Centennial Cone, ^{222}Rn, ^{220}Rn

INTRODUCTION

Samarskite is a complex Nb-Ta-Ti-REE + Y-Ca-U-Th multiple oxide containing uranium, thorium, iron and other elements and has always been found to be completely metamict (Sugitani et al. 1985). Due to its chemical complexity and metamictization, samarskite's chemical formula and crystal structure have not been unambiguously characterized. The proposed structural formulae are: AB_2O_6, $A_3B_5O_{16}$ and ABO_4 where A = REE, U, Th, Ca, Fe and Ti, and B = Nb, Ta and Ti (Komkov 1965; Graham and Thornber 1974; Ewing 1975; Lumpkin et al. 1988). The recently suggested ABO_4 formula is based on microprobe analysis of 19 samarskite samples after annealing at 800^o C under hydrogen and on analysis of samarskite-(Yb) from the Little Patsy pegmatite annealed under a weakly reducing atmosphere at temperatures up to 1100^o C (Warner and Ewing 1993; Simmons et al. 2006).

Radon isotopes ^{222}Rn ($T_{1/2}$ = 3.82 d) and ^{220}Rn ($T_{1/2}$ = 55.6 s) belong to the ^{238}U and ^{232}Th decay series and occur as inert gases. As part of the uranium series, ^{226}Ra decays by α emission (E_α = 4.77 MeV) to form a ^{222}Rn nucleus with an energy of 86 keV. Similarly, ^{224}Ra decays as part of thorium series by α emission (E_α = 5.67 MeV) with a recoil energy of 103 keV for the daughter ^{220}Rn nucleus. Estimated direct recoil lengths for ^{222}Rn and ^{220}Rn within solids typically range from 20-50 nm (Sakoda et al. 2010; Ishimori et al. 2013). For example, the calculated recoil ranges for ^{222}Rn and ^{220}Rn in quartz and zircon are 34 and 38 nm, and 23 and 26 nm, respectively (Sakoda and Ishimori, 2017). These relatively short ranges mean that without internal defects only radon atoms formed near the mineral surface can be detected as emanations (Krupp et al. 2017 and references therein). Emanation coefficients help characterize retention of radon isotopes within mineral matrices. These ratios (reported as percentages) estimate the number of radon or thoron atoms released

from the mineral relative to the number of radon or thoron atoms produced by the decay series occurring within the mineral (Semkow 1990; Morawska and Phillips 1993). Emanation coefficients for metamict minerals can be correlated with uranium and thorium concentrations as well as with their spatial distributions, absorbed α-doses, grain size and nuclear track annealing rates. Emanation coefficients may reflect the extent of structural void space and cracks created by radiation damage from progressive overlap of recoil nuclei cascades of ^{238}U, ^{232}Th and ^{235}U and their daughter products.

Few studies have addressed radon emanations from metamict minerals and only one study has considered radon and thoron emanations from a large sample of samarskite (Malczewski and Dziurowicz 2015). This study analyzes a fragment of the same massive, dark brown, fully metamict specimen of samarskite (SCC; Fig. 1) collected from a granitic pegmatite in Centennial Cone, Jefferson County, Colorado (USA). Table 1 lists basic characteristics of the SCC specimen. According to nomenclature proposed for samarskite-group minerals, the SCC sample described here categorizes as samarskite-(Y) (Hanson et al. 1999; Simmons et al. 2006). As seen in Table 1, the uranium and thorium concentrations correspond to a calculated total absorbed α-dose, D_T, of 6.5 x 10^{17} α-decay mg^{-1}. The α-decays from the ^{238}U and ^{235}U series comprise the dominant contribution to the total α-dose of samarskite from Centennial Cone. The ratio of α-doses from $D_{238} + D_{235}$ to D_{232} is about 27.

The aim of the study is to determine the relationship between ^{222}Rn and ^{220}Rn emanations and annealing temperature for powdered samples of samarskite. Additionally, this work aims to show that ^{222}Rn and ^{220}Rn emanations can be correlated with the thermally induced transition from the low- to high-temperature phase of samarskite. Results obtained are compared with emanation values from a

fragment of the original sample, the unannealed powdered reference sample, and with values from powdered monazite, thorite, uraninite and zircon samples crushed to comparable small grain size as reported from literature sources (Table 2).

MATERIALS AND METHODS

Concentrations of ^{238}U and ^{232}Th were determined from the intact SCC sample using ^{214}Pb and ^{214}Bi (^{238}U), and ^{228}Ac (^{232}Th) gamma-ray activities. Activity concentrations of ^{235}U assumed a natural abundance of ^{238}U/^{235}U = 137.88. Gamma-ray spectra were recorded using a GX3020 system consisting of a coaxial HPGe detector (32% efficiency) in a lead and copper shield (60 mm) with a multichannel buffer (InSpector 2000 DSP). The detector bias voltage was 4000 V and the energy resolution was 0.8 keV at 122 keV and 1.7 keV at 1.33 MeV. Two software packages were used for the efficiency calibration and the determination of radionuclides: LabSOCS (Laboratory Sourceless Calibration Software) and Genie 2000 v.3.4.

After breaking the sample SCC into fragments, 20 pieces of about 2 g were placed in quartz tubes, sealed under argon, and annealed for 1 h and 24 h in a muffle furnace. The temperature program ran from 473 K to 1373 K in increments of 100 K. The furnace stabilized each temperature step within ± 2^{o}. After annealing, the samples were quenched and mechanically ground to an average grain size fraction of 5 μm using an agate ball mill. The original material, crushed to 5 μm grain size but not annealed, is herein designated SRE. The grain sizes were determined for all samples using scanning electron microscopy. Six months after annealing, the powdered samples were placed in copper discs with an outer diameter of 5 cm, an inner diameter of 2 cm, and a 0.15 cm deep groove. The discs were inserted into a stainless steel cylinder (ϕ = 8 cm, h = 3 cm) with two inlets on opposite sides. After insertion, the lid was firmly tightened and inlets were connected to a desiccant and a

RAD7 inlet (Fig. 2). The RAD7 radon system (Durridge Company, Inc.) was used to measure ^{222}Rn and ^{220}Rn emanations. Detailed description of RAD7 electronics and measurement configurations are provided by Durridge Company, Inc. (2000) and in Malczewski and Dziurowicz (2015). The detector operates with a sensitivity of 4 Bq m^{-3}, an upper linear detection limit of 800 kBq m^{-3}, and a manufacturer's calibration accuracy of ± 5%. The drying unit remained open to the ambient air (open loop mode). Measurement for a given powdered sample occurred over a 15 min cycle repeated 10 times for a total run time of 150 min. Each measurement was conducted independently using three RAD7 detectors operating within a temperature range of 20 - 23^{o} C and 4 - 8% internal humidity. The final results represent the average of these three runs. Similar to previous reports (Malczewski and Dziurowicz 2015; Malczewski et al. 2018), the total emission rates for ^{222}Rn (E_{222}) and ^{220}Rn (E_{220}) from the samples were calculated in atoms s^{-1} according to the following equations:

$$E_{222} = \frac{C_{222} \cdot v}{6 \cdot 10^4 \cdot \lambda_{222}} \quad (1)$$

and

$$E_{220} = \frac{1.28 \cdot C_{220} \cdot v}{6 \cdot 10^4 \cdot \lambda_{220}} \quad (2)$$

where C_{222} and C_{220} are respective ^{222}Rn and ^{220}Rn concentrations minus the ambient concentrations (Bq m^{-3}) and v is the flow rate of 1 L min^{-1}. The terms λ_{222} and λ_{220} are respective decay constants for ^{222}Rn and ^{220}Rn of 2.1 x 10^{-6} and 0.012 s^{-1} (Firestone 1996). Our experimental setup (Fig. 2) included a 20 s delay between the emission and measurement by the RAD7 unit. The C_{220} term was therefore multiplied by 1.28.

The ^{222}Rn and ^{220}Rn emanation coefficients (e_{222} and e_{220}, respectively) were calculated as the ratio of ^{222}Rn and ^{220}Rn atoms emitted from a samarskite sample (s^{-1}) and the total amount of ^{222}Rn and ^{220}Rn produced within the sample. Coefficient equations were as follows:

$$e_{222} = \frac{E_{222}}{N_{222}} \quad (3)$$

and

$$e_{220} = \frac{E_{220}}{N_{220}} \quad (4)$$

where N_{222} and N_{220} represent respective estimates of ^{222}Rn and ^{220}Rn nuclei in the sample. Since γ-emitters in both uranium series ($^{234m}Pa \rightarrow {}^{226}Ra \rightarrow {}^{214}Pb \rightarrow {}^{214}Bi$) and thorium series ($^{228}Ac \rightarrow {}^{224}Ra \rightarrow {}^{212}Pb \rightarrow {}^{212}Bi \rightarrow {}^{208}Tl$) were in radioactive equilibrium within the sample analyzed, we assumed that ^{222}Rn and ^{220}Rn values equaled corresponding ^{238}U and ^{232}Th activity concentrations.

Powdered and annealed samarskite samples were also analyzed for their X-ray diffraction (XRD) patterns using a Philips X'Pert diffractometer measuring Cu$K\alpha$ radiation from the Θ-Θ system in scan mode with a 0.02^{o} step size. Figures 3 and 4 show XRD patterns. These figures indicate recrystallization of the fully metamict samarskite SCC begins at 673 K and 573 K for samples subjected to 1 h and 24 h annealing, respectively. The positions of the main diffraction peaks are the same as those reported by Sugitani et al. (1984) for a Kawabe samarskite (Japan) obtained after annealing at 550, 650 and 950^{o} C in a reducing H_2 atmosphere. Sugitani et al. (1984) suggested that the original samarskite phase is formed only under reducing

144 conditions, whereas our results suggest that heating in an inert argon atmosphere
145 also restores metamict samarskite to its original crystalline state.

146 **RESULTS**

147 Table 3 lists the total emission rates and calculated ^{222}Rn and ^{220}Rn
148 emanation coefficients for the unannealed reference sample and samples of
149 samarskite after annealing in argon for 1h (e_{1h222} and e_{1h220}). Table 4 lists the total
150 emission rates and ^{222}Rn and ^{220}Rn emanation coefficients (e_{24h222} and e_{24h220})
151 calculated for samples after 24 h annealing in argon.

152 ***^{222}Rn emanation coefficients versus temperature after 1 h annealing***

153 As shown in Table 3 and Fig. 5, the unheated reference sample (SRE) gave
154 the lowest ^{222}Rn emanation value of 4.9 x 10^{-6} %. For annealed samples, emanation
155 coefficients varied from 5 x 10^{-6} % to 2.1 x 10^{-5} % with an average (arithmetic mean)
156 value of 1.51 x 10^{-5} %. Among annealed samples, those annealed at 973 K (S7) and
157 1073 K (S8) gave the lowest e_{1h222} values of 5 x 10^{-6} % and 9.6 x 10^{-6} %, whereas
158 those annealed at 673 K (S4) and 573 K (S3) gave the highest values of 2.1 x 10^{-5} %
159 and 2 x 10^{-5} %. Figure 5 shows e_{1h222} initially increasing from 473 K to 673 K. At
160 annealing temperatures of 773-873 K, e_{1h222} significantly decreases to a minimum
161 value observed at 973 K (S7). After this point, e_{1h222} values gradually increase up to
162 1373 K (S11).

163 ***^{220}Rn enmanation coefficients versus temperature after 1h annealing***

164 Similar to the ^{222}Rn emanation data, the unheated reference sample (SRE)
165 gave the lowest observed ^{220}Rn emanation value of 3.8 x 10^{-3} % (Tab. 3 and Fig. 6).
166 For annealed samples, ^{220}Rn emanation coefficients (e_{1h220}) ranged from 6.3 x 10^{-3} %
167 to ~2 x 10^{-2} % with an average value of 1.27 x 10^{-2} %. Samples annealed at 973 K

(S7) and 1173 K (S9) gave the lowest e_{1h220} values of 6.3 x 10^{-3} % and 8.4 x 10^{-3} %, whereas those annealed at 1373 K (S11) and 773 K (S5) gave the highest e_{1h220} values of 2 x 10^{-2} % and 1.8 x 10^{-2} %, respectively. As seen in Fig. 6, ^{220}Rn emanation coefficients increase from 473 K to 773 K and then, similar to ^{222}Rn emanation coefficients, rapidly decrease to a minimum at 973 K (S7). At higher temperatures, ^{220}Rn emanation coefficients increase up to a maximum value observed at 1373 K (S11). Variation in ^{220}Rn emanation coefficients with temperature resemble those observed for ^{222}Rn emanation coefficients except for sample S11, which gave the highest e_{1h220} value observed.

^{222}Rn emanation coefficients versus temperature after 24 h annealing

As shown in Table 4 and Fig. 7, and similar to the ^{222}Rn emanation coefficients after 1h annealing, all samarskite samples annealed for 24 h gave higher e_{24h222} values than those of the unannealed reference sample (e_{SRE222}; Tab. 3). The ^{222}Rn emanation coefficients for samples annealed for 24 h ranged from 5.8 x 10^{-6} % to 2.3 x 10^{-5} % with an average value of 1.34 x 10^{-5} %. Samples annealed at 473 K (S12) and 1373 K (S21) gave the lowest e_{24h222} values of 5.8 x 10^{-6} % and 9 x 10^{-6} %, whereas those annealed at at 573 K (S13), 673 K (S14) and 773 K (S15) gave the highest values of 2.3 x 10^{-5} % and 2 x 10^{-5} % (respectively). Figure 7 shows that the e_{24h222} emanation coefficient increases fourfold from sample S12 (473 K) to sample S13 (573 K) and noticeably decreases to a local minimum for sample S17 (973 K). In contrast to the 1h annealing data, e_{24h222} values for samples annealed at the highest temperatures decrease with increasing temperature.

^{220}Rn emanation coefficients versus temperature after 24 h annealing

Similar to the ^{220}Rn emanation coefficients after 1 h annealing, the unheated reference sample (SRE) also gave the lowest ^{220}Rn emanation value after 24 h (Tables 3 and 4 and Fig. 8). For samarskite samples annealed for 24 h, ^{220}Rn emanation coefficients (e_{24h220}) ranged from 4.1 x 10^{-3} % to 1.5 x 10^{-2} % with an average value of 9.87 x 10^{-3} %. Samples annealed at 473 K (S12) and 1073 K (S18) gave the lowest e_{24h220} values of 4.1 x 10^{-3} % and 5.7 x 10^{-3} %, whereas samples annealed at 773 K (S15) and 673 K (S14) gave the highest values of ~1.5 x 10^{-2} % (for both). The ^{220}Rn emanation coefficients increase from 473 K to 773 K and then significantly decrease to a second minimum at 1073 K (S18). The e_{24h220} values increase for samples annealed at 1173 K (S19) and 1273 K (S20), but the e_{24h220} value for sample S21 annealed at 1373 K decrease to 7.4 x 10^{-3} %. Variation in ^{220}Rn emanation coefficients (e_{24h220}) with temperature resembles those observed for ^{222}Rn emanation coefficients (e_{24h222}; Fig. 7) except in the case of sample S18 (1073 K), which exhibited a distinct minimum (Fig. 8).

DISCUSSION

Samples of samarskite annealed for both 1 h and 24 h gave maximum ^{222}Rn emanation coefficients (e_{1h222} and e_{24h222}) within a 573 K to 773 K temperature range. Both datasets also showed a clear minimum at 973 K (Figs. 5 and 7). Samples annealed for 1 h above 973 K gave e_{1h222} values that increase up to 1373 K whereas those annealed for 24 h gave e_{24h222} values that decrease at 1273 K and 1373 K.

Using the analogy of a damped sinusoidal vibration, the variation in all e_{1h222}, e_{24h222}, e_{1h220}, and e_{24h220} emanation coefficients with temperature, after annealing for 1 h and 24 h in argon, can be relatively well fitted using an exponentially decreasing sinusoidal function of the form:

(5)

$$e_i(\%) = e_{0i} + A_i \cdot \exp(-b_i \cdot T) \cdot \sin(c_i \cdot (T - T_{0i}))$$

where e_{0i} is the weighted average of e_i, Ai is the initial amplitude of the envelope, b_i is the damping factor of emanation, and T_{0i} is the temperature at which e_i equals e_{0i}. The term $c_i = \pi / \Delta T_i$, where ΔT_i is the periodicity of e_{0i} and T_{0i}. The index i (i = 1, 2, 3, and 4) refers to e_{1h222}, e_{24h222}, e_{1h220}, and e_{24h220}, respectively. The parameters are explained in Fig. 9, the values of the fitted parameters are listed in Table 5, and the fitted curves are shown in Fig. 10.

The function graphs exhibit two temperature ranges, from 473 K to about 1000 K and from 1000 K to 1373 K, which generally coincide with the recrystallization path proposed by Sugitani et al. (1984). Their research suggested that the low-temperature orthorombic samarskite phase formed after 16 h annealing in H_2 at 550^o C (823 K) and then on heating up to 950^o C (1273 K), at which point a high-temperature monoclinic phase is formed. A splitting of the most intense diffraction peak ($2\Theta \approx 30^o$) into a doublet accompanies the transition from the low- to high-temperature phase. For the Kawabe samarkite, it occurred after heating at 650^o C (923 K), whereas in our study the same main diffraction peak ($2\Theta \approx 30^o$) began splitting at 973 K (Figs. 3 and 4). Warner and Ewing (1993) annealed samarskite samples at 800 ^{o}C (1073 K) in an H_2 atmosphere for 4 h. Those annealed samples were not completely crystalline, which agreed well with our results. Tomašić et al. (2010) analysed a fully metamict samarskite from Beinmyr pegmatite (Norway) annealed in air and Ar/H_2 atmosphere. The high-temperature samarskite phase was not observed at temperatures lower than 800°C (1073 K). The TGA-DTA data for samarskite from Beinmyr recorded from RT (298 K) to 1000°C (1273 K) showed a strong endothermic peak occurring at about 300°C (573 K). This result coincides well

239 with the observation of the highest emanations of ^{222}Rn in a narrow temperature
240 range of 573 to 673 K (Figs. 5 and 7).

241 As shown in Table 5, the calculated b_i values after 24 h annealing, both for
242 $e_{24hh222}$ and e_{24h220}, are about one to two orders of magnitude higher than those for
243 e_{1h222} and e_{1h220} after 1 h annealing. Combined with X-ray patterns, this means that
244 the high-temperature and long-lasting (24 h in this case) annealing lead to the
245 formation of a stable, fully crystalline polymorph of samarskite. As a result, small
246 fluctuations for both $e_{24hh222}$ and e_{24h220} emanation coefficients about their average
247 values are observed (Figs. 10 b and d). After 1 h of annealing, these fluctuations are
248 noticeably higher (Figs. 10 a and c).

249 As seen in Fig. 11, ratios of e_{1h222} to the ^{222}Rn emanation coefficient of the
250 unheated sample (e_{SRE222}) ranged from 1 to 4 with an average 3.1. Ratios of e_{1h222} to
251 the ^{222}Rn emanation coefficient reported for original SCC sample (e_{SCC222}; 1.28 x 10^{-6})
252 varied from 8 to 16 with an average value of 11.8. Ratios corresponding to ^{222}Rn
253 emanation coefficients after 24 h annealing gave similar values. As shown in Fig. 12,
254 the ratio of e_{24h222} to the SRE reference sample emanation coefficient ranged from
255 about 1 to 5 with an average value of 2.7. Ratios of e_{1h222} to the SCC ^{222}Rn
256 emanation coefficient varied from 5 to 18 with an average value of 10.4. Average
257 ^{222}Rn emanation coefficients for samarskite samples ground to a ~5 μm grain size
258 fraction were about two orders of magnitude lower than those reported by Garver and
259 Baskaran (2004) for samples of monazite, zircon, thorite and uraninite, which were
260 crushed to the grain sizes of less than 63 μm and annealed at 873 K for 6 h (Tab. 2).
261 These samples gave ratios of the coefficients from ^{222}Rn emanations after annealing
262 at 873 K to the coefficients from unannealed samples from 0.25 to 0.57, with an
263 average value of 0.4. This value differs from the respective e_{1h222}/e_{SRE222} and

e_{24h222}/e_{SRE222} values of 3.1 and 2.7 reported here. Our results show that annealed samples of samarskite SCC always result in higher values of ^{222}Rn emanation than the unannealed reference sample. A similar effect should be observed for other metamict phases.

The 1.27 x 10^{-2} average value for ^{220}Rn emanation coefficients after 1 h annealing (e_{1h220}) slightly exceeded the 9.87 x 10^{-3} average value calculated for samarskite samples after 24 h annealing (e_{24h220}). Generally, ^{220}Rn emanation coefficients from both 1 h and 24 h annealing exceed ^{222}Rn emanations (e_{1h222} and e_{24h222}) by about three orders of magnitude. Figure 13 shows that ratios of e_{1h220} to the ^{220}Rn emanation coefficient for the unannealed reference sample (e_{SRE220}) range from about 2 to 5 with an average value of 3.3. Ratios of e_{1h220} to the original SCC sample ^{220}Rn emanation coefficient (e_{SCC220} = 3.8 x 10^{-4} %) vary from 17 to 51 with an average value of 33. After 24 h annealing (Fig. 14), ratios of e_{24h220} to the emanation coefficient of the SRE reference sample range from about 1 to 4 with an average value of 2.6. Ratios of e_{24h220} to SCC sample ^{220}Rn emanation coefficients vary from 11 to 40 with an average value of 26. From Figs. 11-14, it appears that the emanation coefficients for both the ^{222}Rn and ^{220}Rn, annealed at temperatures from 473 K to 1373 K, are 3 times higher on average than these observed for the unannealed sample. These figures also show that the emanation coefficients for both ^{222}Rn and ^{220}Rn from samarskite SRE, crushed to 5 μm grain size, exceeded by only one order of magnitude those observed for the intact 4 cm fragment, SCC. A similar effect with reference to granite was reported by Amin and Rama (1986). There was no observed significant difference between radon emanation coefficients from a granite cube with a 30 cm edge and 1-2 mm granite grains.

IMPLICATIONS

289 The observed variations in the ^{222}Rn and ^{220}Rn emanation coefficients with
290 temperature for samples of fully metamict samarskite-(Y) ground to a 5 μm grain size
291 and annealed from 473 K to 1373 K coincide well with the structural conversion from
292 a low- to high-temperature samarskite phase reported in previous studies. The same
293 mineral species showed noticeably different emanation coefficients of radon and
294 thoron depending on the crystallographic system induced by annealing in an argon
295 atmosphere. The ^{222}Rn emanation coefficients obtained both for 1 h and 24 h
296 annealing were significantly lower than the values reported in the literature for
297 comparable metamict minerals. The results reported here indicate that samarskite-
298 (Y) behaves as a closed system for radon retention across a very broad temperature
299 range, from an untreated sample to a sample annealed at 1373 K, despite the high
300 concentration of uranium and unusual structural complexity.

301 **ACKNOWLEDGEMENTS**

302 This work was supported by the National Science Centre, Poland, through grants
303 Nos. 2014/15/B/ST10/04095 and 2018/29/B/ST10/01495. We thank two unknown
304 reviewers for critical comments that improved the final version of this paper.

305 **REFERENCES CITED**

306 Amin, B.S., Rama, (1986) Using radon as probe for investigating characteristic of
307 fractures in crystalline materials. Nuclear Instruments and Methods in Physics
308 Research B, 17, 527-529.

309 Bryant, B., McGrew, L.W., and Wobus, R.A. (1981) Geologic map of the Denver 1 x 2
310 degree quadrangle, north-central Colorado: U.S. Geological Survey Miscellaneous
311 Investigations Map I-1163, scale 1:250,000.

312 Durridge Company Inc. (2000) RAD7 Radon Detector. Part No. 1280, Bedford, MA.

Ewing, R.C. (1975) The crystal chemistry of complex niobium and tantalum oxides. IV. The metamict state: Discussion. American Mineralogist, 60, 728-733.

Firestone, R.B. (Ed.) (1996) Table of isotopes. Wiley-Interscience, Lawrence Berkeley National Laboratory.

Garver, E., and Baskaran, M. (2004) Effects of heating on the emanation rates of radon-222 from a suite of natural minerals. Applied Radiation and Isotopes, 61, 1477-1485.

Graham, J., and Thornber, M.R. (1974) The crystal chemistry of complex niobium and tantalum oxides I. Structural classification of MO_2 phases. American Mineralogist, 59, 1026-1039.

Hanson, S.L., Simmons, W.B., Falster, A.U., Foord, E.E., and Lichte, F.E. (1999) Proposed nomenclature for samarskite-group minerals: new data on ishikawaite and calciosamarskite. Mineralogical Magazine, 61(1), 27-36.

Ishimori, Y., Lange K., Martin, P., Mayya, Y.S., and Phaneuf (2013) Measurement and calculation of radon releases from NORM residues. International Atomic Energy Agency (IAEA).Technical Reports Series No. 474.

Komkov, A.I. (1965) Crystal structure and chemical constitution of samarskite. Doklady Akademiia Nauk SSSR, Earth Science Section, 160, 127-129. (English translation).

Krupp, K., Baskaran, M., and Brownlee, S.J. (2017) Radon emanation coefficients of several minerals: How they vary with physical and mineralogical properties. American Mineralogist, 102, 1375-1383.

Lumpkin, G.R., Ewing, R.C., and Eyal, Y. (1988) Preferential leaching and natural annealing of alpha-recoil tracks in metamict betafite and samarskite. Journal of Materials Research, 3(2), 357-368.

Malczewski, D., and Dziurowicz, M. (2015) 222Rn and 220Rn emanations as a function of the absorbed α-doses from select metamict minerals. American Mineralogist, 100, 1378-1385.

Malczewski, D., and Dziurowicz, M., Krzykawski, T., and Stryjewski, A. (2018) 222Rn and 220Rn emanations from zircon crystals as a function of absorbed α-doses. The Canadian Mineralogist, 56, 451-462.

Morawska, L., and Phillips, C.R. (1993) Dependence of the radon emanation coefficient on radium distribution and internal structure of the material. Geochimica et Cosmochimica Acta, 57, 1783-1797.

Sakoda, A., Hanamoto, K., Ishimori, Y., Kataoka, T., Kawabe, A., and Yamaoka, K. (2010) First model of the effect of grain size on radon emanation. Applied Radiation and Isotopes, 68, 1169-1172.

Sakoda, A., and Ishimori, Y. (2017) Mechanism and Modelling Approaches of Radon Emanation for Natural Materials. Japanese Journal of Health Physics, 52(4), 296-306.

Semkow, T.M. (1990) Recoil-emanation theory applied to radon release from mineral grains. Geochimica et Cosmochimica Acta, 54, 425-440.

Simmons, W.B., Hanson, S.L., and Falster, A.U. (2006) Samarskite-(Yb): A new species of the samarskite group from the Little Patsy Pegmatite, Jefferson County, Colorado. The Canadian Mineralogist, 44, 1119-1125.

Sugitani, Y., Suzuki, Y., and Nagashima, K. (1984) Recovery of the original samarskite structure in a reducing atmosphere. American Mineralogist, 69, 377-379.

Sugitani, Y., Suzuki, Y., and Nagashima, K. (1985) Polymorphism of samarskite and its ralationship to other structurally related Nb-Ta oxides with the α-PbO_2 structure. American Mineralogist, 70, 856-866.

Tomašić, N., Gajović, A., Bermanec, V., Linarić, M.R., Su, D., and Škoda, R. (2010) Preservation of the samarskite structure in a metamict ABO_4 mineral: a key to crystal structure identification. European Journal of Mineralogy, 22, 435-442.

Warner, J.K., and Ewing, R.C. (1993) Crystal chemistry of samarskite. American Mineralogist, 78, 419-424.

Figure captions

FIGURE 1.

Photo of fully metamict samarskite (SCC) from Centennial Cone, Colorado, USA. The specimen is 4 cm in length. About half of the specimen was used in this study.

FIGURE 2.

Experimental setup for measuring ^{222}Rn and ^{220}Rn emanations from powdered samarskite samples.

FIGURE 3.

X-ray diffraction (XRD) patterns for the unheated SRE samarkite sample and samples after 1 h annealing under argon from 473 K (S2) to 1373 K (S11).

FIGURE 4.

X-ray diffraction (XRD) patterns for samarskite samples after 24 h annealing under argon from 473 K (S12) to 1373 K (S21).

FIGURE 5.

^{222}Rn emanation coefficients for unheated SRE samarskite sample (e_{SRE222}) and for samples after 1 h annealing in argon (e_{1h222}) from 473 K to 1373 K.

FIGURE 6.

^{220}Rn emanation coefficients for unheated SRE samarskite sample (e_{SRE220}) and for samples after 1 h annealing in argon (e_{1h220}) from 473 K to 1373 K.

FIGURE 7.

^{222}Rn emanation coefficients for unheated SRE samarskite sample (e_{SRE222}) and for samples after 24 h annealing in argon (e_{24h222}) from 473 K to 1373 K.

FIGURE 8.

^{220}Rn emanation coefficients for unheated SRE samarskite sample (e_{SRE220}) and for samples after 24 h annealing in argon (e_{24h220}) from 473 K to 1373 K.

FIGURE 9.

The parameters used in this work to describe variations in the ^{222}Rn and ^{220}Rn emanation coefficients with temperature, based on Eq. (5).

FIGURE 10.

Plots of **(a)** e_{1h222}, **(b)** e_{24h222}, **(c)** e_{1h220}, and **(d)** e_{24h220} versus temperature. The solid lines show the fit to the experimental data based on Eq. (5). Thin horizontal lines represent the fitted values of e_{0i}.

FIGURE 11.

Plot of ratios of ^{222}Rn emanations from samarskite samples after 1 h annealing (e_{1h222}) to ^{222}Rn emanation from unheated reference sample (e_{SRE222}) (circles) and ratios of e_{1h222} to ^{222}Rn emanation from original sample (e_{SCC222}) (triangles) versus temperature. Thin solid line shows average e_{1h222} / e_{SRE222} ratio and thick solid line shows average e_{1h222} / e_{SCC222} ratio.

FIGURE 12.

Plot of ratios of ^{222}Rn emanations from samarskite samples after 24 h annealing (e_{24h222}) to ^{222}Rn emanation from unheated reference sample (e_{SRE222}) (circles), and ratios of e_{24h222} to ^{222}Rn emanation from original large sample e_{SCC222} (triangles) versus temperature. Thin solid line shows average e_{24h222} / e_{SRE222} ratio and thick solid line shows average e_{24h222} / e_{SCC222} ratio.

FIGURE 13.

Plot of ratios of ^{220}Rn emanations from samarskite samples after 1 h annealing (e_{1h220}) to ^{220}Rn emanation from unheated reference sample (e_{SRE220}) (squares) and ratios of e_{1h220} to ^{220}Rn emanation from original sample (e_{SCC220}) (inverted triangles) versus temperature. Thin solid line shows average e_{1h220} / e_{SRE220} ratio and thick solid line shows average e_{1h220} / e_{SCC220} ratio.

FIGURE 14.

Plot of ratios of ^{220}Rn emanations from samarskite samples after 24 h annealing (e_{24h220}) to ^{220}Rn emanation from unheated reference sample (e_{SRE220}) (squares) and ratios of e_{24h220} to ^{220}Rn emanation from original sample (e_{SCC220}) (inverted triangles) versus temperature. Thin solid line shows average e_{24h220} / e_{SRE220} ratio and thick solid line shows average e_{24h220} / e_{SCC220} ratio.

428

This is a preprint, the final version is subject to change, of the American Mineralogist (MSA)
Cite as Authors (Year) Title. American Mineralogist, in press.
DOI: https://doi.org/10.2138/am-2020-6988

Table 1

Age, basic chemical composition (wt.%), calculated absorbed α-doses and ^{222}Rn and ^{220}Rn emanation coefficients for the original intact samarskite sample (SCC).

Age	1550(150) Ma[a]
O	20.12(81)
Si	2.39(10)
Ca	2.0(1)
Ti	1.78(10)
Fe	2.83(15)
Y	7.17(32)
Nb	29.05(64)
Ta	5.19(54)
Pb	2.69(56)
Th	1.82(2)
U	10.54(40)
Calculated total dose (D_T)[b] (α-decay mg^{-1})	6.5 x 10^{17}
Calculated dose from ^{232}Th (D_{232}) (α-decay mg^{-1})	2.3 x 10^{16}
Calculated dose from ^{238}U (D_{238}) (α-decay mg^{-1})	5.77 x 10^{17}
Calculated dose from ^{235}U (D_{235}) (α-decay mg^{-1})	4.97 x 10^{16}
e_{SCC222}[c]	1.28 x 10^{-6}%
e_{SCC220}	3.8 x 10^{-4}%

[a] Bryant et al (1981). [b] Doses were calculated as: $D_{238} = 8 \times N_{238}(e^{t\lambda,238} - 1)$, $D_{235} = 7 \times N_{235}(e^{t\lambda,235} - 1)$, $D_{232} = 6 \times N_{232}(e^{t\lambda,232} - 1)$ and $D_T = D_{238} + D_{235} + D_{232}$. N_{238}, N_{235} and N_{232} are the present number of atoms of ^{238}U, ^{235}U and ^{232}Th per milligram, λ_{238}, λ_{235} and λ_{232} are the decay constants of ^{238}U, ^{235}U and ^{232}Th (respectively), and t is the geologic age. The absorbed ^{235}U α-doses were calculated assuming a natural atomic abundance of ^{238}U/^{235}U = 137.88. [c] ^{222}Rn emanation coefficient (e_{222}) and ^{220}Rn emanation coefficient (e_{220})

This is a preprint, the final version is subject to change, of the American Mineralogist (MSA)
Cite as Authors (Year) Title. American Mineralogist, in press.
DOI: https://doi.org/10.2138/am-2020-6988

Table 2

Previously reported ^{222}Rn emanation coefficients for metamict minerals crushed to grain size of less than 63 μm and heated for 6 h (Garver and Baskaran 2004).

Sample	**Heating temperature (K)**	**e_{222} (%)**	**e_{600}/e_{RT}**
Monazite	RT	2.05	
	873	0.66	0.32
Zircon	RT	1.04	
	873	0.47	0.45
Uraninite	RT	0.53	
	873	0.30	0.57
Thorite	RT	5.38	
	873	1.34	0.25
		Average	0.40

This is a preprint, the final version is subject to change, of the American Mineralogist (MSA)
Cite as Authors (Year) Title. American Mineralogist, in press.
DOI: https://doi.org/10.2138/am-2020-6988

Table 3

Total emission rates and ^{222}Rn and ^{220}Rn emanation coefficients for the samarskite samples after 1 h annealing and for unheated reference sample (SRE).

Annealing temperature (K)	**Sample**	**N_{222} (10^8 atoms)**	**E_{222} (atom s^{-1})**	**e_{1h222} (%)[a]**	**N_{220} (10^3 atoms)**	**E_{220} (atom s^{-1})**	**e_{1h220} (%)[b]**
RT	SRE	7.26	35.6	4.90×10^{-6}	7.23	0.27	3.76×10^{-3}
473	S2	4.91	56.1	1.14×10^{-5}	4.89	0.46	9.46×10^{-3}
573	S3	2.93	58.9	2.01×10^{-5}	2.92	0.30	1.02×10^{-2}
673	S4	4.95	102	2.07×10^{-5}	4.93	0.83	1.69×10^{-2}
773	S5	4.91	93.3	1.90×10^{-5}	4.89	0.88	1.79×10^{-2}
873	S6	6.04	112	1.86×10^{-5}	6.02	0.82	1.36×10^{-2}
973	S7	6.96	35	5.04×10^{-6}	6.94	0.44	6.34×10^{-3}
1073	S8	5.69	54.9	9.65×10^{-6}	5.67	0.53	9.34×10^{-3}
1173	S9	4.75	65	1.37×10^{-5}	4.74	0.37	8.36×10^{-3}
1273	S10	5.29	83.5	1.58×10^{-5}	5.27	0.79	1.49×10^{-2}
1373	S11	4.98	87.2	1.75×10^{-5}	4.97	0.98	1.97×10^{-2}
Average				1.51×10^{-5}			1.27×10^{-2}

[a] Estimated uncertainties $\Delta e_{222}/e_{222} \leq 14\%$. [b] Estimated uncertainties $\Delta e_{220}/e_{220} \leq 10\%$.

This is a preprint, the final version is subject to change, of the American Mineralogist (MSA)
Cite as Authors (Year) Title. American Mineralogist, in press.
DOI: https://doi.org/10.2138/am-2020-6988

Table 4

Total emission rates and ^{222}Rn and ^{220}Rn emanation coefficients for samarskite samples after 24 h annealing.

Annealing temperature (K)	Sample	N_{222} (10^8 atoms)	E_{222} (atom s^{-1})	e_{24h222} (%)[a]	N_{220} (10^3 atoms)	E_{220} (atom s^{-1})	e_{24h220} (%)[b]
473	S12	6.81	39.7	5.82×10^{-6}	6.79	0.28	4.14×10^{-3}
573	S13	3.29	75.3	2.29×10^{-5}	3.28	0.45	1.37×10^{-2}
673	S14	3.49	69.2	1.98×10^{-5}	3.48	0.51	1.46×10^{-2}
773	S15	4.91	96.1	1.96×10^{-5}	4.89	0.74	1.52×10^{-2}
873	S16	5.21	60.1	1.16×10^{-5}	5.19	0.65	1.04×10^{-2}
973	S17	5.69	54.5	9.56×10^{-6}	5.67	0.50	8.83×10^{-3}
1073	S18	7.57	93.2	1.23×10^{-5}	7.54	0.43	5.74×10^{-3}
1173	S19	3.98	49.4	1.24×10^{-5}	3.96	0.37	9.20×10^{-3}
1273	S20	4.70	50.4	1.07×10^{-5}	4.68	0.45	9.51×10^{-3}
1373	S21	6.48	58.6	9.02×10^{-6}	6.46	0.48	7.40×10^{-3}
Average				1.34×10^{-5}			9.87×10^{-3}

[a] Estimated uncertainties $\Delta e_{222}/e_{222} \leq 14\%$. [b] Estimated uncertainties $\Delta e_{220}/e_{220} \leq 10\%$.

This is a preprint, the final version is subject to change, of the American Mineralogist (MSA)
Cite as Authors (Year) Title. American Mineralogist, in press.
DOI: https://doi.org/10.2138/am-2020-6988

Table 5

Fitted parameters for the function given by Eq. (5).

i	**1**	**2**	**3**	**4**
Parameter	$\mathbf{e_{1h222}}$	$\mathbf{e_{24h222}}$	$\mathbf{e_{1h220}}$	$\mathbf{e_{24h220}}$
e_{0i} (%)	1.37×10^{-5}	1.17×10^{-5}	1.24×10^{-2}	9.1×10^{-3}
A_i	1.48×10^{-5}	3.27×10^{-4}	6.1×10^{-3}	6.9×10^{-2}
b_i (K^{-1})	6.8×10^{-4}	5.3×10^{-3}	9.8×10^{-5}	3.9×10^{-3}
T_{0i} (K)	506	504	547	520
ΔT_i (K)	339	346	342	415
Adj. R^2	0.82	0.81	0.78	0.76

* Individual uncertainties estimated for parameters are ≤ 20%

FIGURE 1

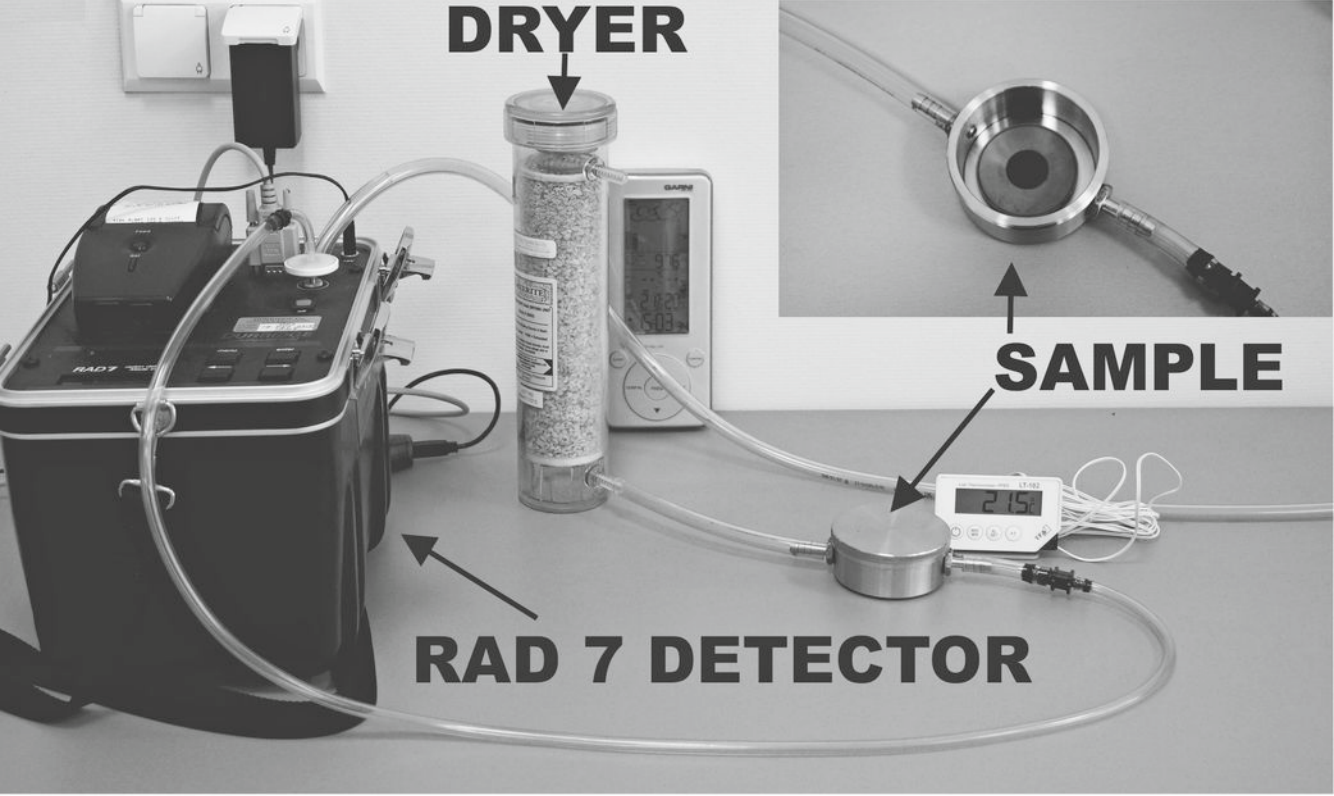

FIGURE 2

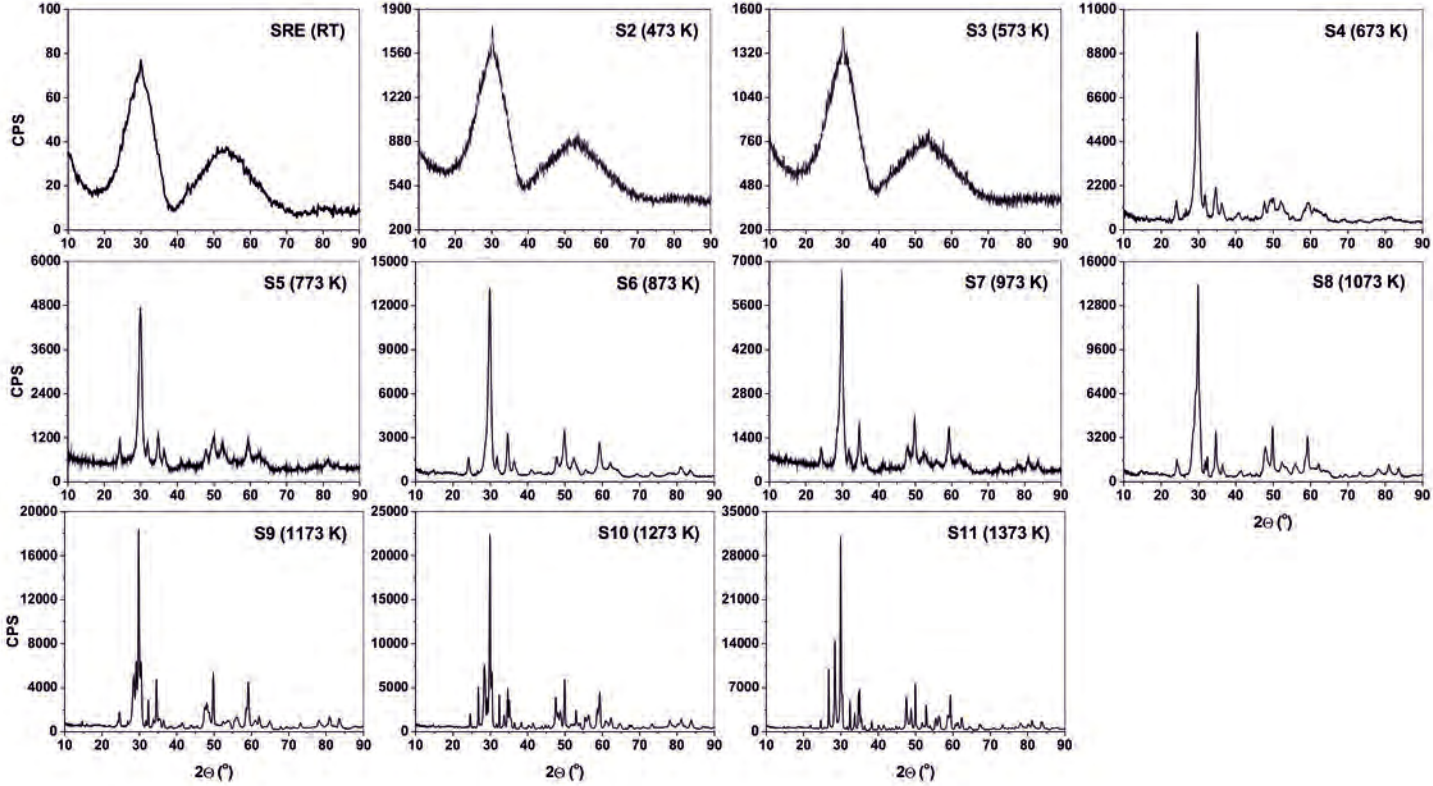
SRE (RT)
S2 (473 K)
S3 (573 K)
S4 (673 K)
S5 (773 K)
S6 (873 K)
S7 (973 K)
S8 (1073 K)
S9 (1173 K)
S10 (1273 K)
S11 (1373 K)
CPS
2Θ (°)

FIGURE 3

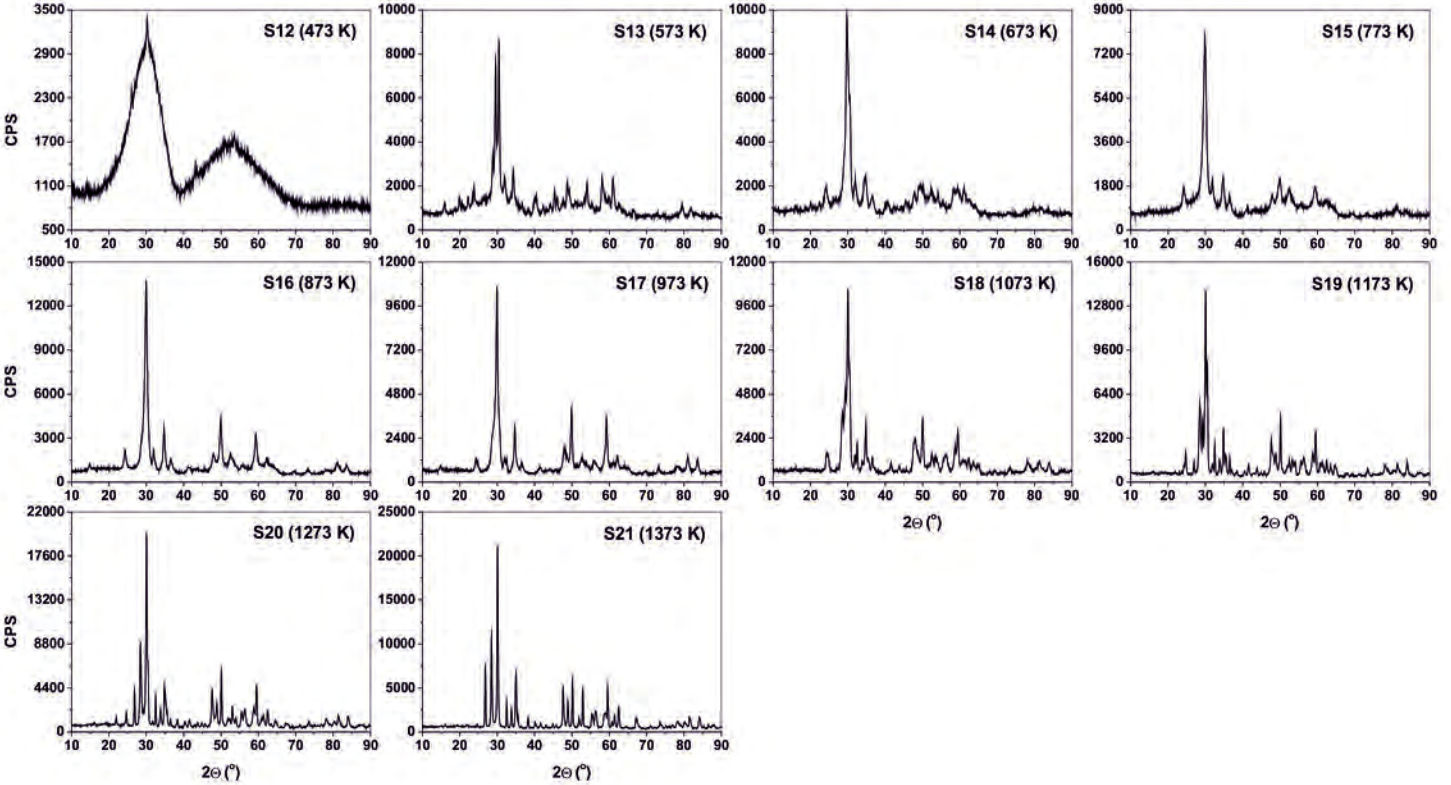
S12 (473 K)
S13 (573 K)
S14 (673 K)
S15 (773 K)
S16 (873 K)
S17 (973 K)
S18 (1073 K)
S19 (1173 K)
S20 (1273 K)
S21 (1373 K)
CPS
2Θ (°)

FIGURE 4

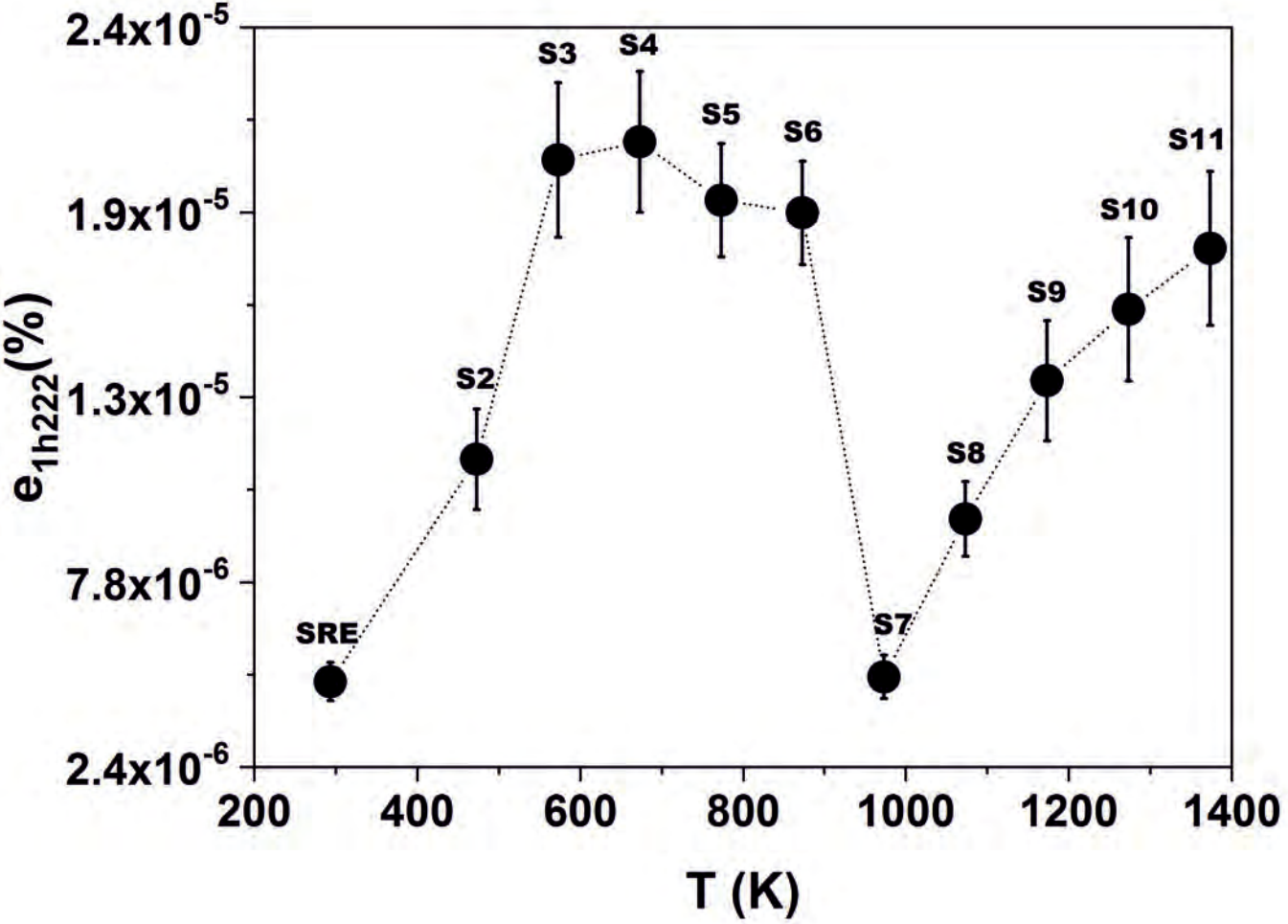
2.4x10-5
1.9x10-5
1.3x10-5
7.8x10-6
2.4x10-6
e1h222(%)
SRE
S2
S3
S4
S5
S6
S7
S8
S9
S10
S11
200
400
600
800
1000
1200
1400
T (K)

FIGURE 5

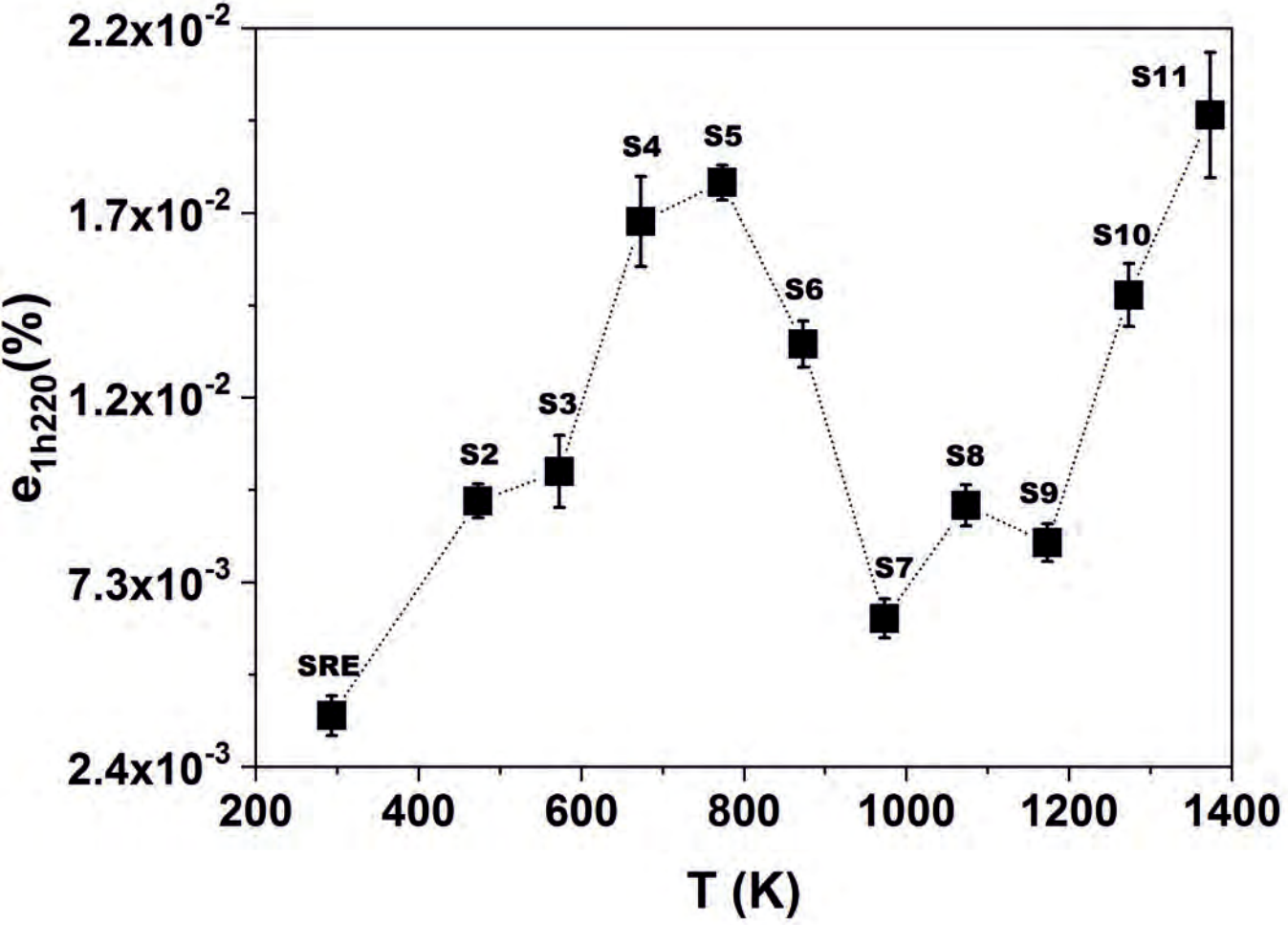
2.2x10-2
1.7x10-2
1.2x10-2
7.3x10-3
2.4x10-3
e1h220(%)
200
400
600
800
1000
1200
1400
T (K)
SRE
S2
S3
S4
S5
S6
S7
S8
S9
S10
S11

FIGURE 6

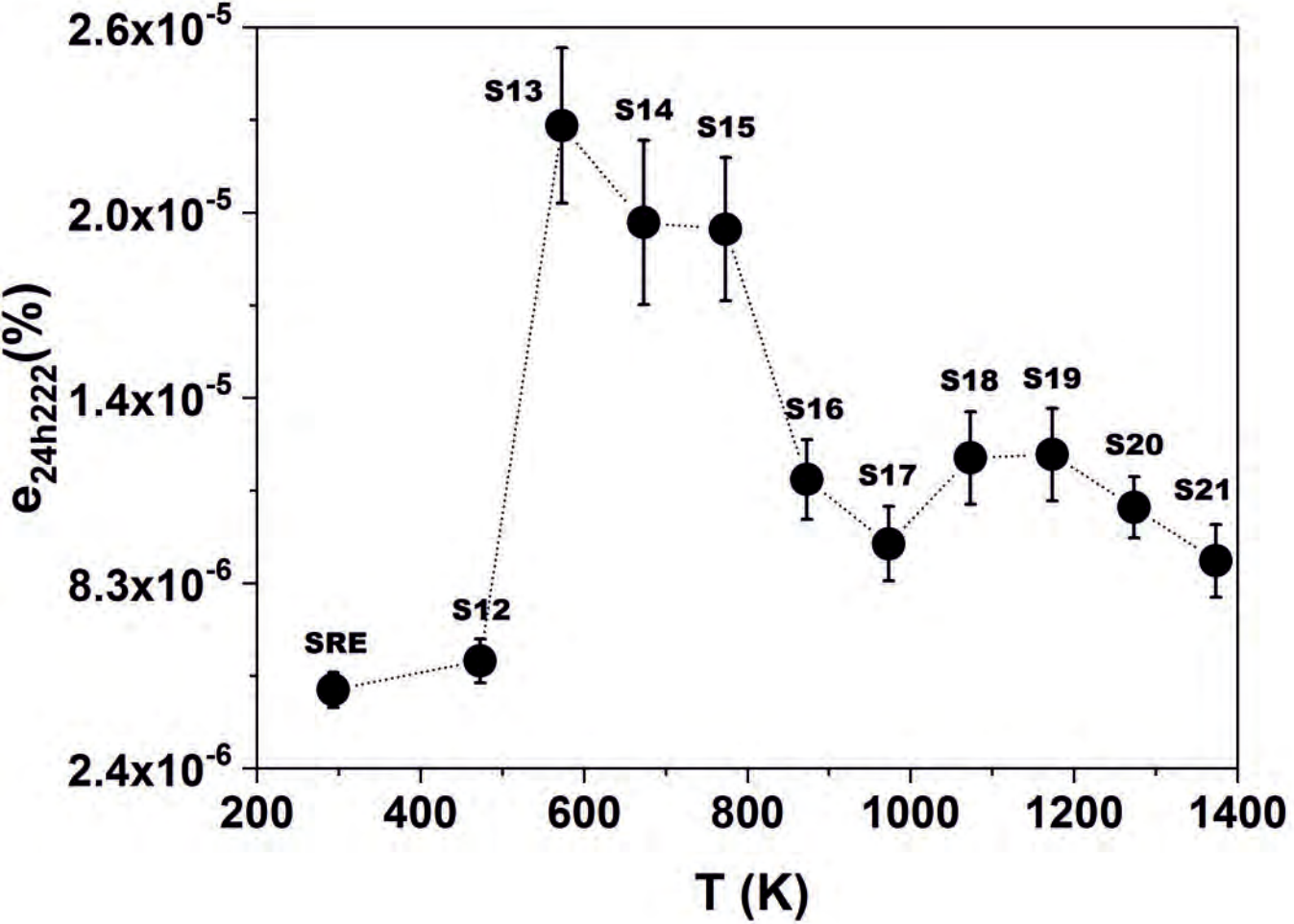
2.6x10-5
2.0x10-5
1.4x10-5
8.3x10-6
2.4x10-6
e24h222(%)
200
400
600
800
1000
1200
1400
T (K)
SRE
S12
S13
S14
S15
S16
S17
S18
S19
S20
S21

FIGURE 7

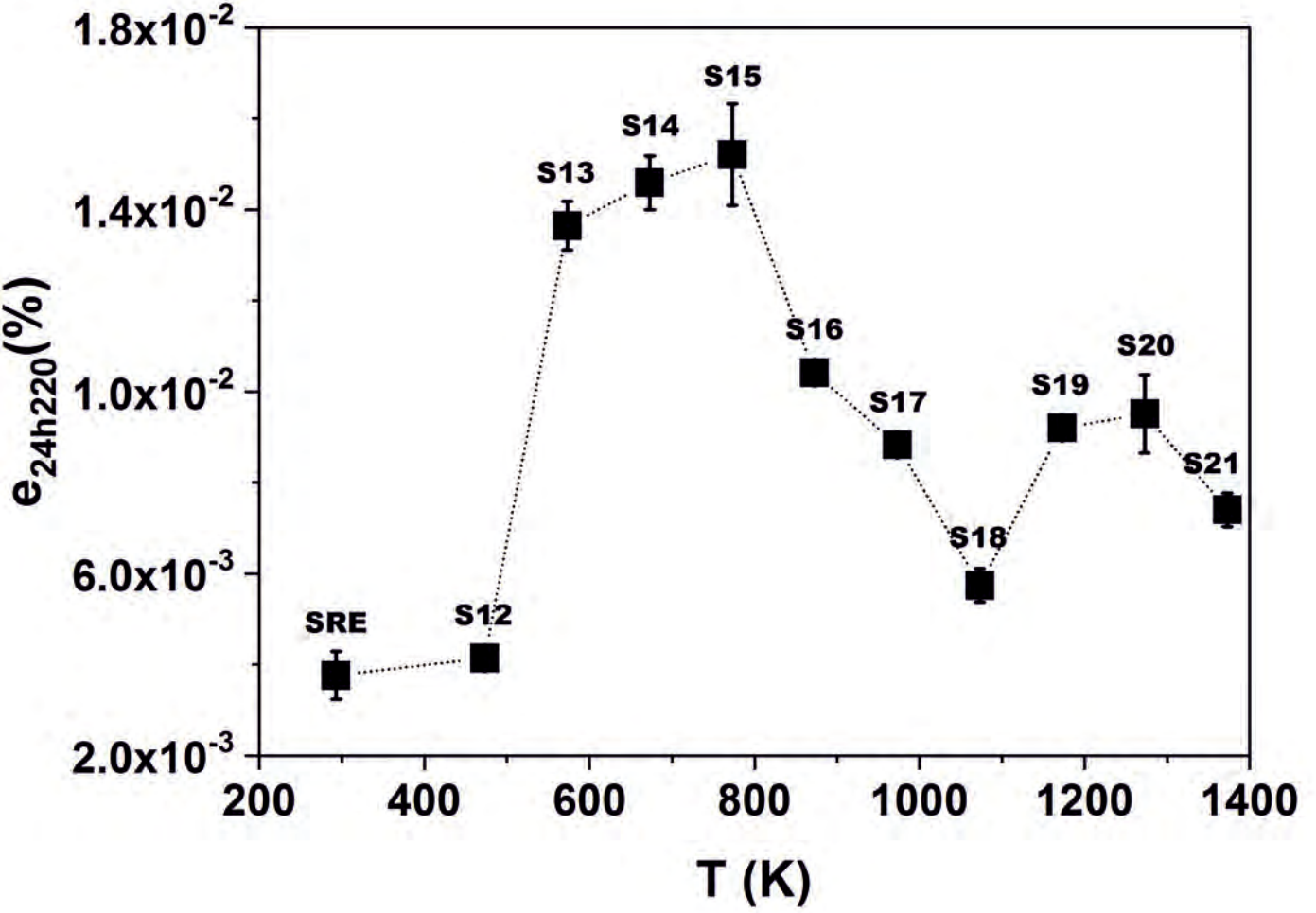
1.8x10-2
1.4x10-2
1.0x10-2
6.0x10-3
2.0x10-3
e24h220(%)
200
400
600
800
1000
1200
1400
T (K)
SRE
S12
S13
S14
S15
S16
S17
S18
S19
S20
S21

FIGURE 8

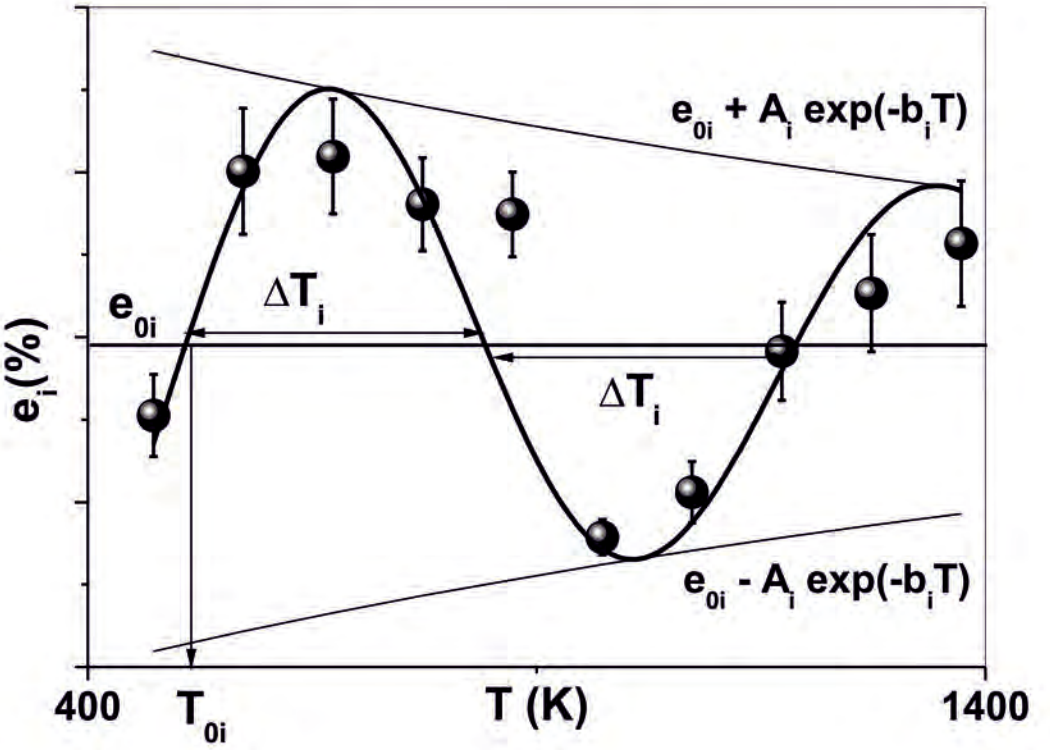

FIGURE 9

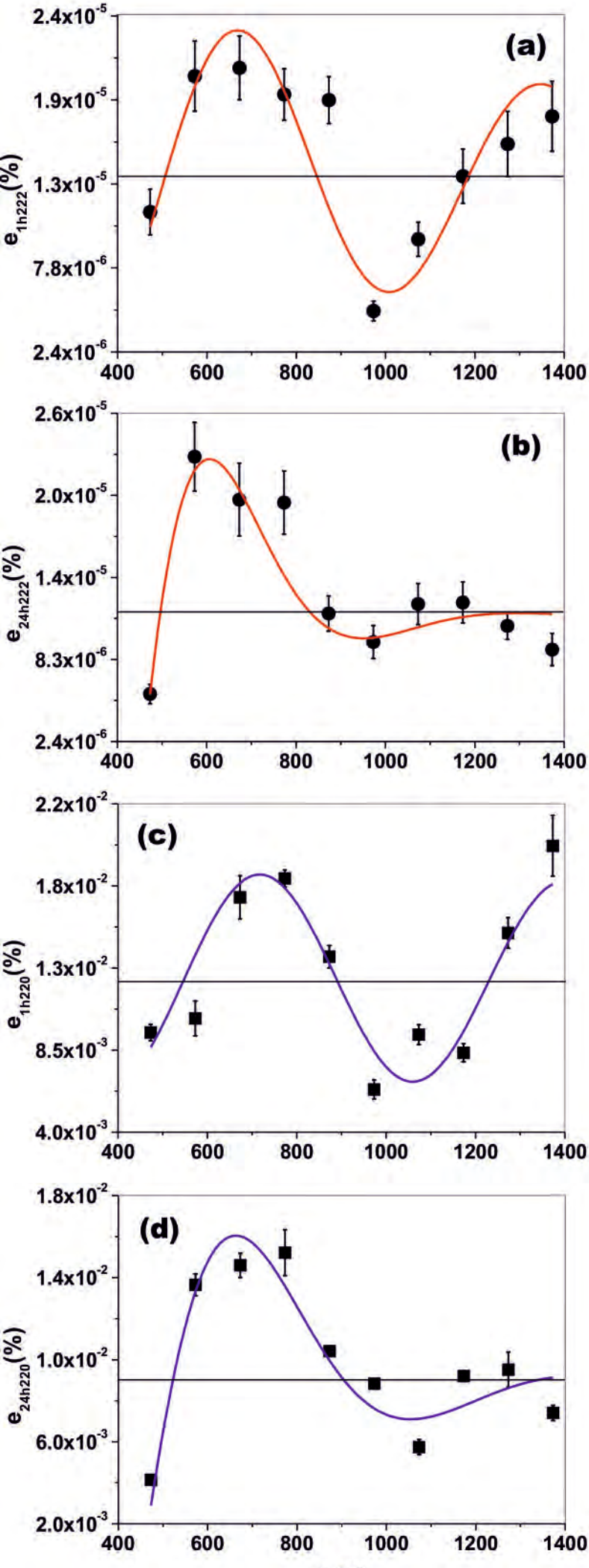
(a)
(b)
(c)
(d)
e_{1h222}(%)
e_{24h222}(%)
e_{1h220}(%)
e_{24h220}(%)
2.4x10^{-5}
1.9x10^{-5}
1.3x10^{-5}
7.8x10^{-6}
2.4x10^{-6}
2.6x10^{-5}
2.0x10^{-5}
1.4x10^{-5}
8.3x10^{-6}
2.4x10^{-6}
2.2x10^{-2}
1.8x10^{-2}
1.3x10^{-2}
8.5x10^{-3}
4.0x10^{-3}
1.8x10^{-2}
1.4x10^{-2}
1.0x10^{-2}
6.0x10^{-3}
2.0x10^{-3}
400
600
800
1000
1200
1400
T (K)

FIGURE 10

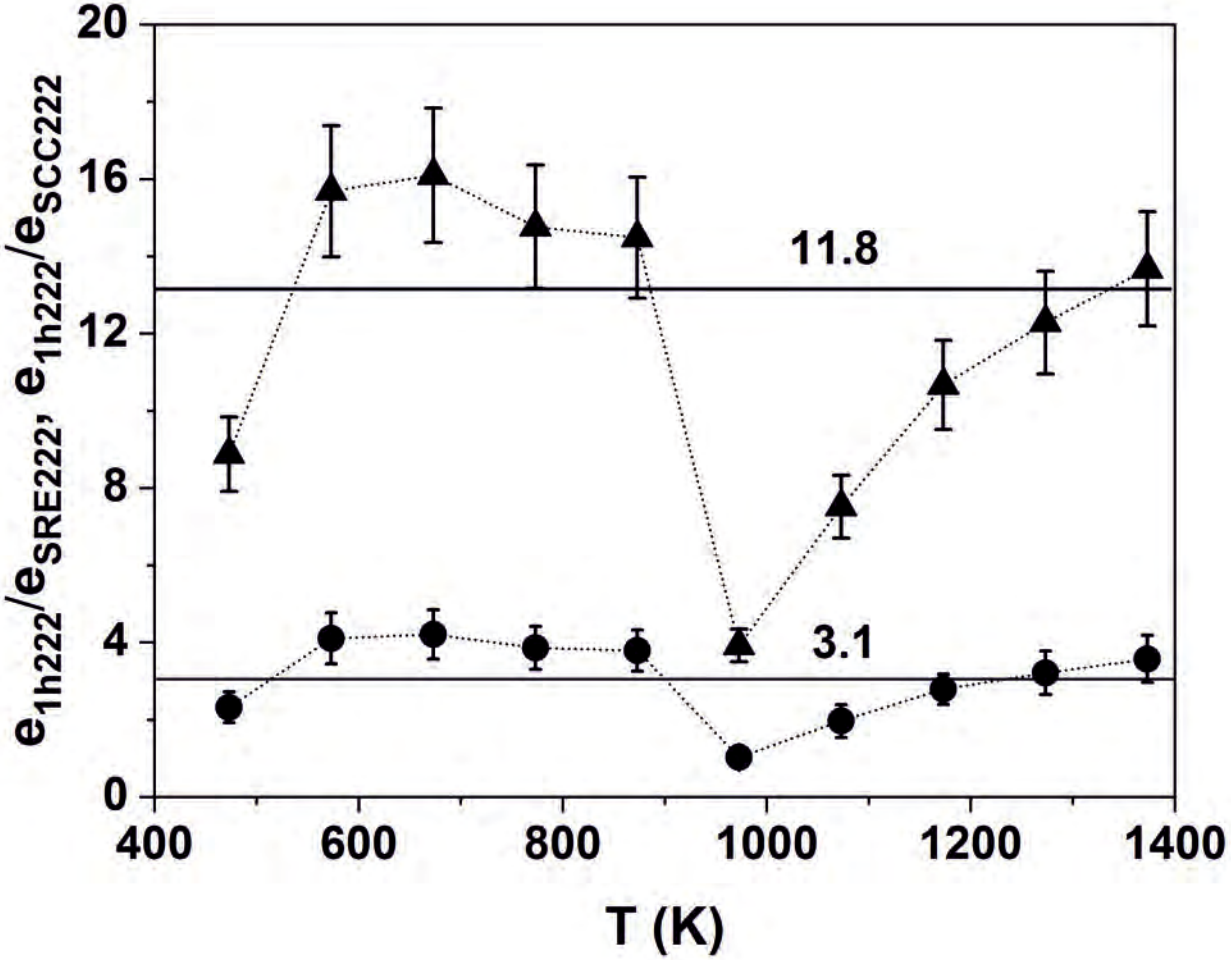
20
16
12
8
4
0
400
600
800
1000
1200
1400
T (K)
e_{1h222}/e_{SRE222}, e_{1h222}/e_{SCC222}
11.8
3.1

FIGURE 11

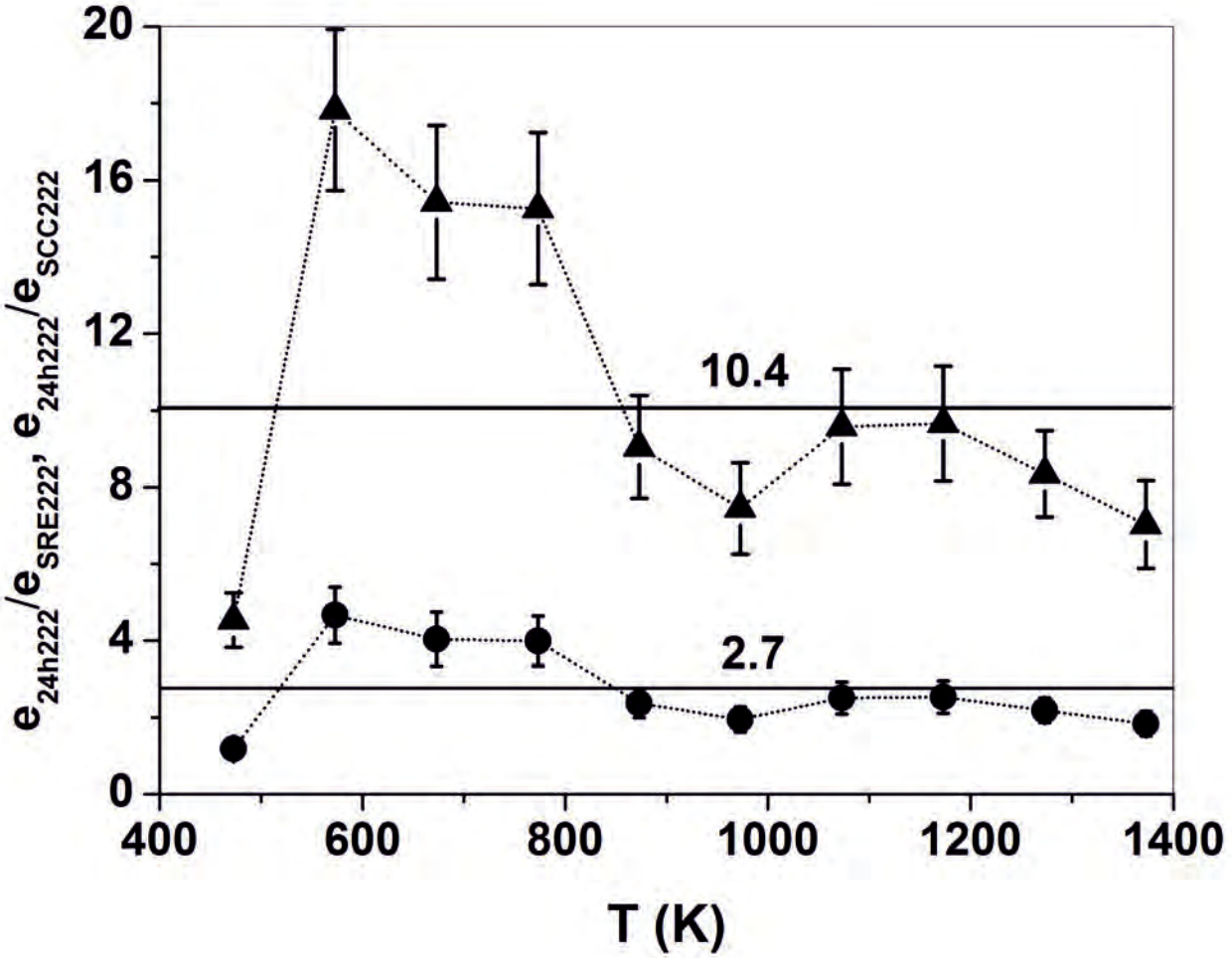
20
16
12
8
4
0
400
600
800
1000
1200
1400
T (K)
e_{24h222}/e_{SRE222}, e_{24h222}/e_{SCC222}
10.4
2.7

FIGURE 12

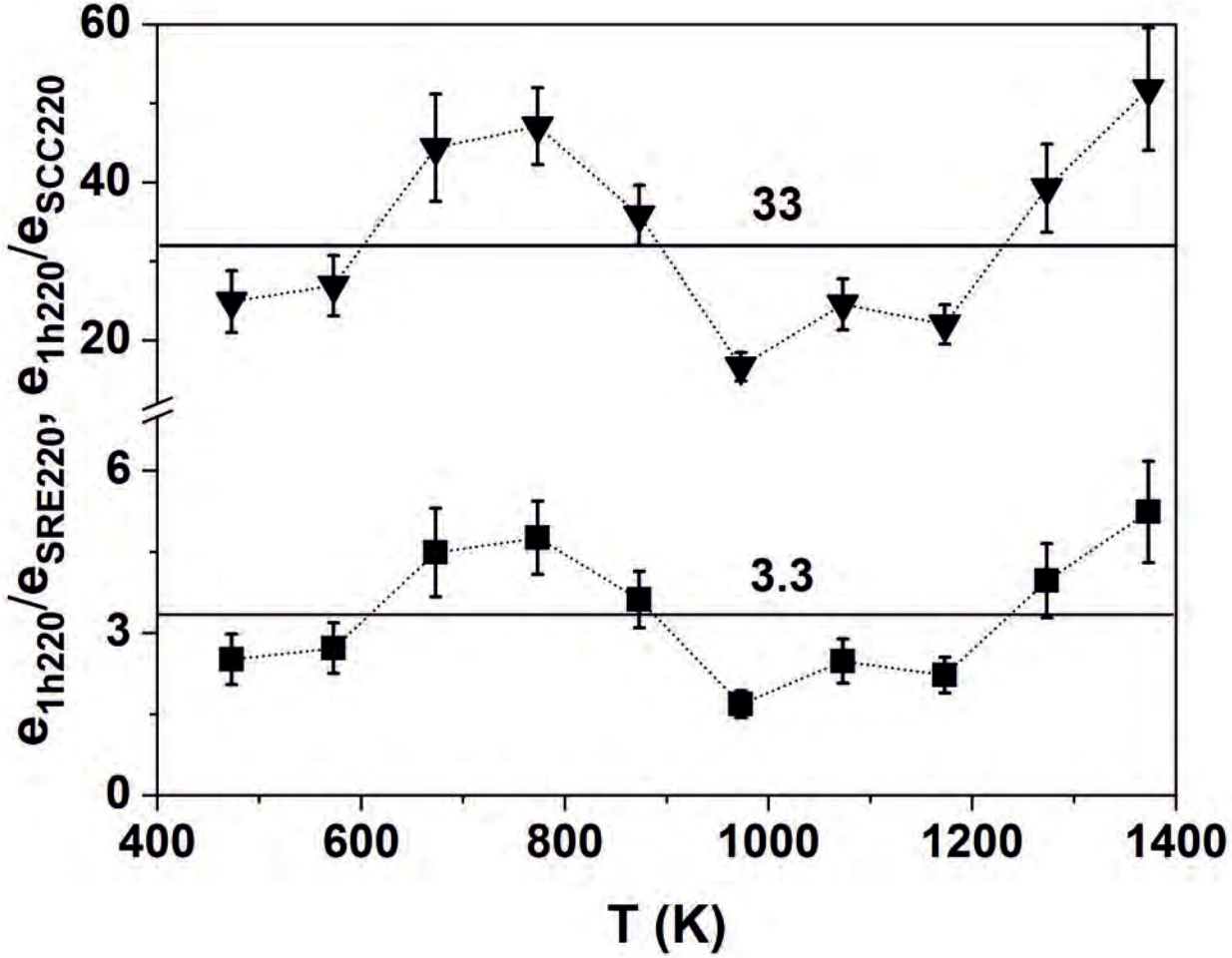
60
40
20
6
3
0
400
600
800
1000
1200
1400
T (K)
33
3.3
e1h220/eSRE220, e1h220/eSCC220

FIGURE 13

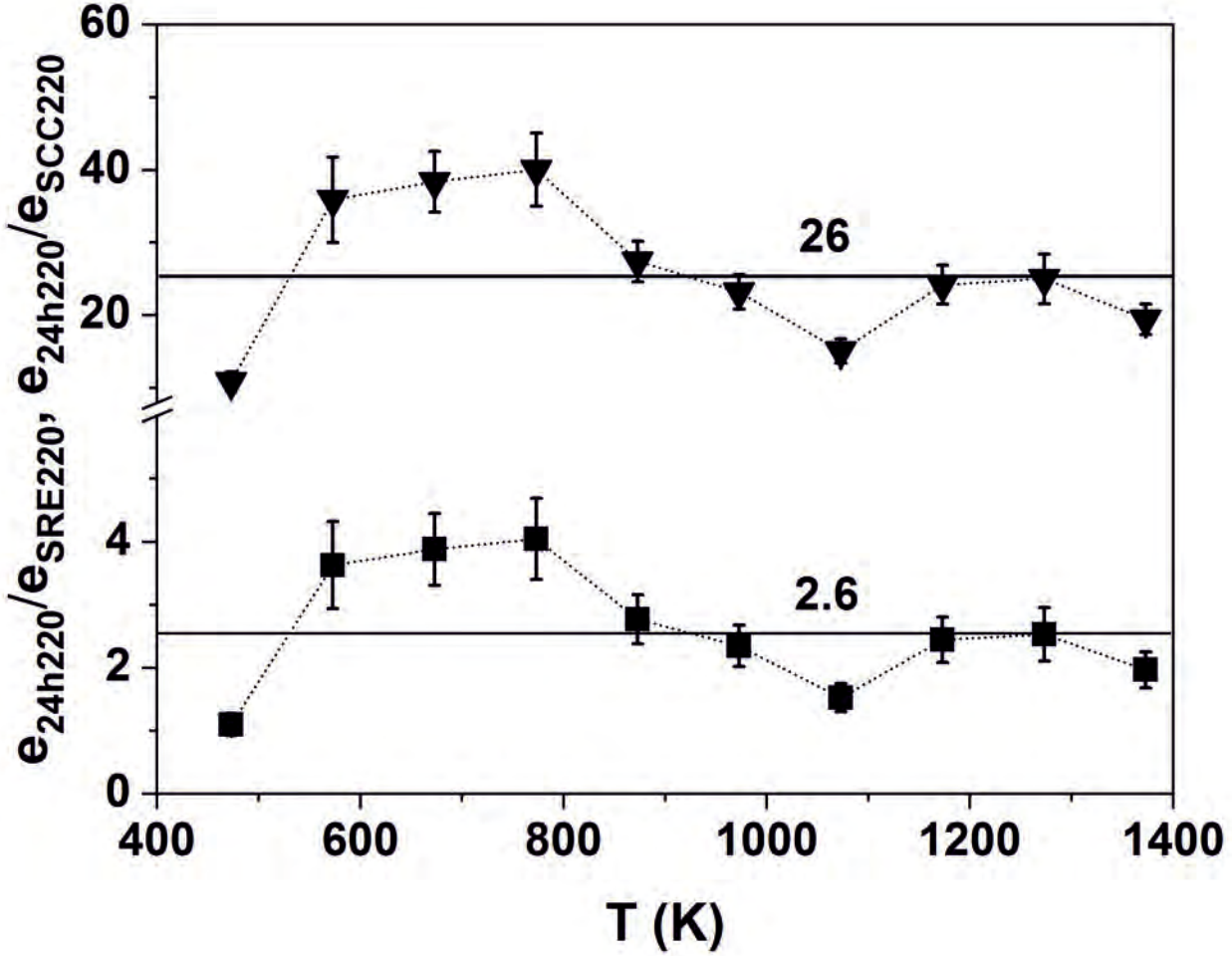
60
40
20
4
2
0
400
600
800
1000
1200
1400
26
2.6
T (K)
e24h220/eSRE220, e24h220/eSCC220

FIGURE 14